7-5-2016

Evidence That the P_i Release Event Is the Rate-Limiting Step in the Nitrogenase Catalytic Cycle

Zhi-Yong Yang
Utah State University

Rhesa Ledbetter
Utah State University

Sudipta Shaw
Utah State University

Natasha Pence
Montana State University-Bozeman

Monika Tokmina-Lukaszewska
Montana State University-Bozeman

See next page for additional authors

Accepted version. *Biochemistry,* Vol. 55, No. 26 (July 5, 2016): 3625-3635. DOI.

Authors
Zhi-Yong Yang, Rhesa Ledbetter, Sudipta Shaw, Natasha Pence, Monika Tokmina-Lukaszewska, Brian Eilers, Qingjuan Guo, Nilisha Pokhrel, Valerie L. Cash, Dennis R. Dean, Edwin Antony, Brian Bothner, John W. Peters, and Lance C. Seefeldt

Evidence That the Pi Release Event Is the Rate-Limiting Step in the Nitrogenase Catalytic Cycle

Zhi-Yong Yang
Department of Chemistry and Biochemistry, Utah State University, Logan, Utah
Rhesa Ledbetter
Department of Chemistry and Biochemistry, Utah State University, Logan, Utah
Sudipta Shaw
Department of Chemistry and Biochemistry, Utah State University, Logan, Utah
Natasha Pence
Department of Chemistry and Biochemistry, Montana State University, Bozeman, Montana

Biochemistry, Vol 55, No. 26 (July 5, 2016): pg. 3625-3635. DOI.

Monika Tokmina-Lukaszewska
Department of Chemistry and Biochemistry, Montana State University, Bozeman, Montana
Brian Eilers
Department of Chemistry and Biochemistry, Montana State University, Bozeman, Montana
Qingjuan Guo
Department of Chemistry and Biochemistry, Utah State University, Logan, Utah
Nilisha Pokhrel
Department of Biological Sciences, Marquette University, Milwaukee, Wisconsin
Valerie L. Cash
Department of Biochemistry, Virginia Tech, Blacksburg, Virginia
Dennis R. Dean
Department of Biochemistry, Virginia Tech, Blacksburg, Virginia
Edwin Antony
Department of Biological Sciences, Marquette University, Milwaukee, Wisconsin
Brian Bothner
Department of Chemistry and Biochemistry, Montana State University, Bozeman, Montana
John W. Peters
Department of Chemistry and Biochemistry, Montana State University, Bozeman, Montana

Biochemistry, Vol 55, No. 26 (July 5, 2016): pg. 3625-3635. DOI.

Lance C. Seefeldt

Department of Chemistry and Biochemistry,
Utah State University,
Logan, Utah

Abstract

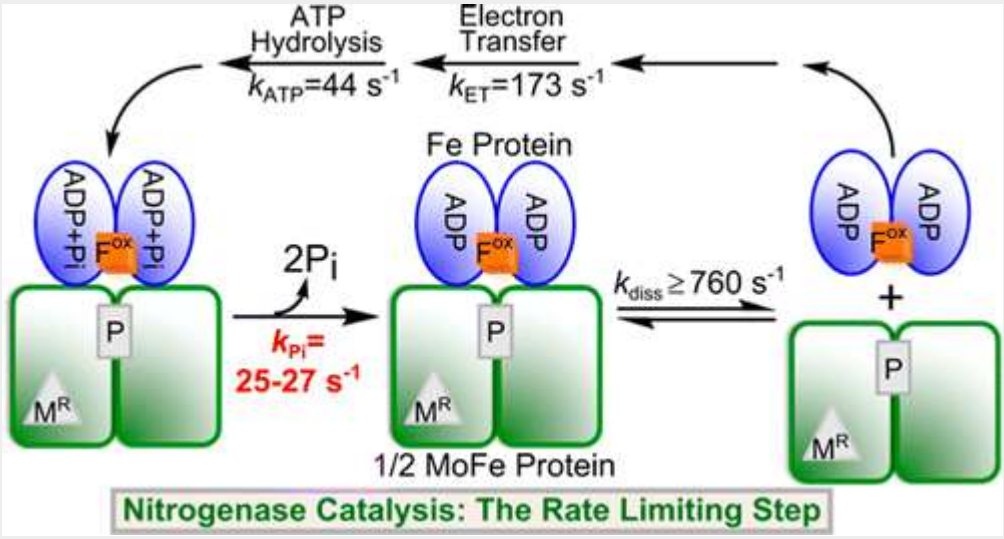

Nitrogenase reduction of dinitrogen (N_2) to ammonia (NH_3) involves a sequence of events that occur upon the transient association of the reduced Fe protein containing two ATP molecules with the MoFe protein that includes electron transfer, ATP hydrolysis, P_i release, and dissociation of the oxidized, ADP-containing Fe protein from the reduced MoFe protein. Numerous kinetic studies using the nonphysiological electron donor dithionite have suggested that the rate-limiting step in this reaction cycle is the dissociation of the Fe protein from the MoFe protein. Here, we have established the rate constants for each of the key steps in the catalytic cycle using the physiological reductant flavodoxin protein in its hydroquinone state. The findings indicate that with this reductant, the rate-limiting step in the reaction cycle is not protein–protein dissociation or reduction of the oxidized Fe protein, but rather events associated with the P_i release step. Further, it is demonstrated that (i) Fe protein transfers only one electron to MoFe protein in each Fe protein cycle coupled with hydrolysis of two ATP molecules, (ii) the oxidized Fe protein is not reduced when bound to MoFe protein, and (iii) the Fe protein interacts with flavodoxin using the same binding interface that is used with the MoFe protein. These findings allow a revision of the rate-limiting step in the nitrogenase Fe protein cycle.

Nitrogenase is the catalyst responsible for biological nitrogen fixation, the reduction of dinitrogen (N_2) to ammonia (NH_3).[1-3] The molybdenum-dependent nitrogenase consists of two catalytic components called the MoFe protein and the Fe protein.[4] The Fe protein is a dimer of two identical subunits connected by a single [4Fe-4S] cluster and is responsible for transferring a single electron to the MoFe protein.[5, 6] The MoFe protein is a heterotetramer, composed of two symmetric αβ units. Each αβ unit contains two unique metal clusters, the electron carrier P-cluster [8Fe-7S] and the active site FeMo cofactor [7Fe-9S–Mo–C-homocitrate].[7-11] An Fe protein, with two bound MgATP molecules, binds transiently to each αβ unit of the MoFe protein during the electron transfer (ET) event (Figure 1).[6, 12, 13] ET is initiated upon association of the Fe protein with the MoFe protein, followed by a conformationally gated one-electron transfer from the P-cluster to the FeMo cofactor.[14, 15] This is followed by the one-electron transfer from the reduced Fe protein (Fe^{red}) [4Fe-4S] cluster to the oxidized P-cluster (P^{1+}), in what has been called a "deficit spending" ET process.[14] Following ET, the two ATP molecules are hydrolyzed to two ADP molecules and two P_i molecules. Next, the two P_i molecules are released from the complex, followed by the dissociation of the oxidized Fe protein (Fe^{ox}) with two bound MgADP molecules [$Fe^{ox}(ADP)_2$] from the MoFe protein.[16] The $Fe^{ox}(ADP)_2$ is then reduced by a reductant, and the two ADP molecules are replaced by two ATP molecules.[17, 18] This cycle, often termed the Fe protein cycle, must be repeated a sufficient number of times to cause the accumulation of the electrons necessary for substrate reduction in the MoFe protein.[1-3, 18-20]

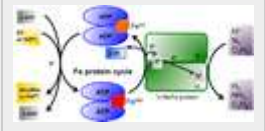

Figure 1. Overview of nitrogenase catalysis with a focus on the Fe protein cycle showing dithionite (DT) and flavodoxin (Fld^{HQ}) as a nonphysiological reductant and a physiological reductant, respectively.

Over the past five decades, most of the *in vitro* mechanistic studies of nitrogenase have been conducted with the nonphysiological reductant dithionite (DT), largely because of ease of use.[1, 3, 18] The kinetic parameters for each step in the Fe protein cycle using DT as a reductant have been deduced and are summarized in the scheme

Biochemistry, Vol 55, No. 26 (July 5, 2016): pg. 3625-3635. DOI.

shown in Figure 2.[16-18, 21, 22] It was concluded from a comparison of the rate constants that the overall rate-limiting step in the Fe protein cycle is the dissociation of $Fe^{ox}(ADP)_2$ from the MoFe protein with a rate constant of ~6 s^{-1}.[16, 17] A problem that is often overlooked in such studies is the reversible dissociation of DT ($S_2O_4^{2-}$) to generate the actual reductant, the radical anion $SO_2^{\bullet-}$, with a K_d of ~1.5 nM and a slow rate constant of ~2 s^{-1}.[17] This leads to slow reduction of Fe^{ox}, with rate constants for this reduction near the rate constant that is reported for dissociation of $Fe^{ox}(ADP)_2$ from MoFe protein.[16, 17, 22, 23]

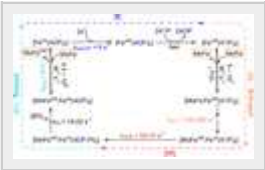

Figure 2. Fe protein cycle with pseudo-first-order kinetic rate constants for each step.

The physiological reductants of Fe protein are known to be the electron carrier proteins flavodoxin (Fld) and ferredoxin (Fd).[24-30] Because nitrogenase is readily reduced by artificial electrons donors, such as DT, a limited number of kinetic studies using physiological reductants have been conducted.[24, 25, 27, 30-35] The diazotroph *Azotobacter vinelandii* contains several Flds and Fds. NifF (Fld) has been implicated as an electron donor to nitrogenase[26, 29, 30, 36] and has been shown to transfer electrons to Fe protein *in vitro*.[24, 25, 27, 33, 34] Further, disruption in the *nif*F gene results in a 30% decrease in whole-cell acetylene reduction activity. This previous research demonstrates that Fld is a major, but not the sole, electron donor to nitrogenase.[26, 29] Fld has three different redox states designated as the oxidized quinone (Fld^{Q}), one-electron-reduced semiquinone (Fld^{SQ}), and two-electron-reduced hydroquinone (Fld^{HQ}).[24, 37, 38] The pH- and temperature-dependent midpoint redox potentials (E_m) for the two redox couples are estimated to be −180 mV (vs the NHE) for the Fld^{Q}/Fld^{SQ} couple and −480 mV for the Fld^{SQ}/Fld^{HQ} couple (pH 8.5 and 22 °C).[38] The Fld^{SQ}/Fld^{HQ} redox couple has sufficient driving force for reduction of the oxidized Fe protein with a midpoint potential of −290 mV without nucleotide bound and −440 mV with ADP bound.[25, 27, 33, 34, 39] Earlier kinetic studies using Fld as a reductant have yielded results that contradict some aspects of the Fe protein cycle deduced with DT.

Biochemistry, Vol 55, No. 26 (July 5, 2016): pg. 3625-3635. DOI.

(i) The one-electron reduction of Fe protein by Fld^{HQ} is much faster than that by DT, and this reduction event might happen when $Fe^{ox}(ADP)_2$ is still bound to the MoFe protein.[25] (ii) Fe protein can be reduced by two electrons by Fld^{HQ} to an all ferrous state, possibly allowing two electrons to be transferred per two ATP molecules hydrolyzed (a 1:1 ATP:e^- ratio).[33, 34] (iii) In the Fe protein cycle, the dissociation step might be faster than what has been widely accepted ($\sim$6 s^{-1}).[25, 31-33, 40]

In this work, kinetic studies were performed using both DT and Fld (NifF from *A. vinelandii*) as reductants to deduce the key kinetic parameters in the Fe protein cycle. This work reveals that Fld^{HQ} cannot reduce the Fe protein while it is bound to MoFe protein, the ratio of the number of ATP molecules hydrolyzed per electron transferred remains at 2:1 for a wide range of substrates, and the rate-limiting step in the Fe protein cycle is not the dissociation of the Fe protein from the MoFe protein, but rather events associated with P_i release.

Materials and Methods

General Procedures

All chemicals, unless otherwise noted, were obtained from Sigma-Aldrich (St. Louis, MO) and used without further purification. Hydrogen, acetylene, ethylene, argon, and dinitrogen gases were purchased from Air Liquide America Specialty Gases LLC (Plumsteadville, PA). The argon and dinitrogen gases were passed through an activated copper catalyst to remove dioxygen contamination prior to use. *A. vinelandii* strains DJ995 (wild-type MoFe protein) and DJ884 (wild-type Fe protein) were grown, and nitrogenase proteins were expressed and purified as previously described.[41] Both proteins were greater than 95% pure as confirmed by sodium dodecyl sulfate–polyacrylamide gel electrophoresis (SDS–PAGE) analysis using Coomassie blue staining and fully active (see Results and Discussion). Proteins and buffers were handled anaerobically in septum-sealed serum vials under an inert atmosphere (argon or dinitrogen), on a Schlenk vacuum line, or anaerobic glovebox (MO-10-M, Teledyne Analytical Instruments, Hudson, NH). The transfer of gases and liquids was done with gastight syringes.

Biochemistry, Vol 55, No. 26 (July 5, 2016): pg. 3625-3635. DOI.

Strain Construction and Expression, Escherichia coli Growth, and NifF Purification

The *nif*F gene from *A. vinelandii* was amplified via polymerase chain reaction and cloned into the NdeI–BamHI sites of a T7-7 plasmid containing an ampicillin resistance gene for selection. Fld was overexpressed in *E. coli* BL21 DE3 cells. The cells were grown to an optical density (600 nm) of 0.6–0.8 at 37 °C before protein expression was induced at 32 °C by adding isopropyl β-D-1-thiogalactopyranoside (IPTG) and flavin mononucleotide (FMN) to final concentrations of 1 mM and 10 mg/L, respectively. Following a 10 h induction, cells were harvested.

All steps during the purification of Fld were conducted anaerobically under an argon atmosphere; 100 g of cell paste was resuspended in 50 mM Tris (pH 8) with 2 mM dithiotheritol (DTT) at a biomass:buffer ratio of 1:5 (w/v). The resuspended cells were lysed in a French pressure cell (SLM Aminco FA-078, Aminco, Rochester, NY) at 200 MPa. The cell lysate was centrifuged (Sorvall Lynx 4000, ThermoScientific, Waltham, MA) at 48000*g* for 30 min at 4 °C. Following centrifugation, 0.5% (w/v) streptomycin sulfate was added to the supernatant to precipitate nucleic acids. The precipitation was removed via a second centrifugation as described above. The supernatant was loaded onto a 150 mL Q-Sepharose column, which was first washed with 2 column volumes of buffer B [50 mM Tris, 1 M NaCl, and 1 mM DTT (pH 8)] and then equilibrated with 2 column volumes of buffer A [50 mM Tris and 1 mM DTT (pH 8)]. A 15 to 75% salt gradient was run over 5 column volumes. Fractions containing Fld (blue color) were combined and diluted with buffer A to a final NaCl concentration of <100 mM. FMN was added to a final concentration of 2 mM to increase the percentage of holo-Fld in the presence of 2 mM DT, which slowly changed the color of the protein solution from blue to yellow. The reconstitution was conducted for at least 2 h at room temperature. The protein was then loaded onto a Q-Sepharose column (~30 mL) prereduced and equilibrated with buffer B and buffer A containing 1 mM DT. After being loaded, the column was washed with 1 column volume of buffer A and eluted with 100% buffer B as a concentrated fraction for loading onto the Sephacryl-200 column (~600 mL) equilibrated with 100 mM HEPES (pH 7.8) with 150 mM NaCl, 0.5 mM DTT, and 1 mM DT. The Fld was followed as a yellow-

Biochemistry, Vol 55, No. 26 (July 5, 2016): pg. 3625-3635. DOI.

green band. The protein was concentrated using an Amicon (EMD Millipore, Billerica, MA) concentrator with a 10000 kDa cutoff membrane and stored in liquid nitrogen. The purity of the Fld was greater than 95% based on the SDS–PAGE method described above. The FMN content was determined to be ~70% of the total protein. This was determined by measuring the absorbance of Fld^{Q} at 452 nm and using an extinction coefficient of 11.3 mM^{-1} $cm^{-1.37}$ The Fld concentration used in this work refers to the concentration of the holo-Fld with FMN bound.

Steady-State Substrate Reduction Assays for Determination of k_{cat} for Fe Protein and MoFe Protein

Substrate reduction assays were conducted in 9.4 mL sealed serum vials with a liquid volume of 1 mL in an assay buffer consisting of an MgATP regeneration system (5 mM $MgCl_2$, 22 mM phosphocreatine, 4 mM ATP, 0.2 mg/mL creatine phosphokinase, and 1 mg/mL BSA) in 100 mM MOPS buffer (pH 7.3) with 10 mM DT or a 600 μM Fld^{HQ}/10–12 mM DT mixture. After solutions were made anaerobic, the headspace in the reaction vials was adjusted to proper partial pressures for the various gaseous substrates, such as acetylene and N_2. The MoFe protein was then added to the designated final concentration. Each reaction vial was preincubated in a 30 °C water bath for 1 min before initiation of the reaction by the addition of Fe protein. Reaction mixtures were incubated for 30 s at 30 °C with a shaking rate of 130 rpm before the reactions were quenched by the addition of 500 μL of 400 mM EDTA at pH 8.0 or 500 μL of 1 M formic acid. The products (H_2, C_2H_4, and NH_3) from different substrate reduction assays were quantified according to published methods.[42] Refer to substrate reduction tables and figures for detailed information about assay conditions and concentrations.

Determination of ATP/e^- Values for Different Substrate Reduction Reactions

The total number of electrons transferred for product formation (H_2, C_2H_4, and NH_3) from different substrate reduction reactions was determined. The reaction mixture contained 8.5 mM ATP, 9.7 mM $MgCl_2$, and 1 mg of BSA in 100 mM MOPS buffer (pH 7.3) with either 10 mM DT or a 712 μM Fld^{HQ}/10 mM DT mixture. General substrate

reduction assay procedures are described above. To quantify the amount of hydrolyzed ATP as formation of ADP, a trace amount of [α-^{32}P]ATP at a final concentration of ~0.006 μM was added to the reaction mixture. The reactions were then initiated by addition of a mixture of MoFe and Fe protein at a designated molar ratio. A 25 μL aliquot was removed from the mixture and the reaction quenched with 50 μL of 1 M formic acid. One microliter of the quenched mixture was spotted onto a silicon-gel thin-layer chromatography (TLC) plate and developed in 0.6 M potassium phosphate buffer (pH 3.4) for 70 min. The plate was dried and exposed overnight to a phosphor screen. The [α-^{32}P]ATP and [α-^{32}P]ADP were detected with a Storm PhosphorImager and quantified using the ImageQuant software (Molecular Dynamics). The amount of hydrolyzed ATP or produced ADP was quantified on the basis of the density ratio of [α-^{32}P]ATP and [α-^{32}P]ADP spots from each experiment after subtracting no protein controls.

Stopped-Flow (SF) Spectrophotometry and Reduction of Fe Protein by DT and Fld^{HQ}

SF spectrophotometry was conducted using an AutoSF-120 stopped-flow instrument equipped with a data acquisition system (KinTek Corp., Snow Shoe, PA). The change in absorbance was monitored at 426 nm over time. This wavelength detects a decrease in absorbance as the Fe protein [4Fe-4S] cluster becomes reduced. A wavelength of 426 nm rather than 430 nm was chosen because the former is the isosbestic point of Fld (Figure S6). Reactions were conducted at 4 °C, unless otherwise stated, with a mixing ratio of 1:1. All samples were prepared in 100 mM MOPS buffer (pH 7.3). Fe protein was oxidized in an anaerobic glovebox using an ~3-fold molar excess of phenazine methosulfate (PMS). The protein/PMS mixture was allowed to incubate for 15 min prior to separation with Sephadex G-25 equilibrated with 100 mM MOPS (pH 7.3) with 150 mM NaCl. The oxidized Fe protein was contained in one drive syringe with or without nucleotide. The other drive syringe contained the electron donor, DT or Fld^{HQ}/DT mixture, with or without nucleotide. All reagents were used at the following final concentrations and kept under an argon atmosphere: 40 μM oxidized Fe protein, 10 mM DT, 300 μM Fld, 10 mM ATP or ADP, and 10 mM $MgCl_2$ (used only in the presence of nucleotides). For the reduction of Fe^{ox} by DT, the data were fit to a

single-exponential equation to obtain the pseudo-first-order rate constants. Because of the presence of both Fld^{HQ} and DT in the experiments, the pseudo-first-order rate constants for reduction of Fe^{ox} by Fld^{HQ} were obtained by fitting the data to a double-exponential equation.

Reduction of $Fe^{ox}(ADP)_2$ by Different Reductants in the Presence of MoFe Protein

The Fe–MoFe dissociation rate constant was determined using SF as described above except that the temperature was 25 °C. Fe protein was oxidized (see details above), and MoFe protein was stripped of DT in an anaerobic glovebox. DT was removed from MoFe protein using a DOWEX-Sephadex G-25 column equilibrated with 100 mM MOPS (pH 7.3) containing 150 mM NaCl. One drive syringe contained 80 μM Fe^{ox}, 80 μM MoFe protein, and 9 mM MgADP. The other syringe contained the reductant mixture: (1) 20 mM DT, (2) 100 μM methyl viologen (MV)/20 mM DT mixture, or (3) 400 μM Fld^{HQ}/20 mM DT mixture. All reductants contained 9 mM MgADP. DT data were fit to a single-exponential decay equation, and MV/DT and Fld^{HQ}/DT data were fit to a double-exponential decay equation.

Primary Electron Transfer

Primary electron transfer from the Fe protein to the MoFe protein in the presence of DT and Fld was measured at 25 °C using SF spectrophotometry as described above. All mixtures were prepared in 100 mM MOPS (pH 7.3) and kept under an argon atmosphere. One syringe contained 80 μM Fe protein, 20 μM MoFe protein, and 1 mM DT with or without 200 μM Fld^{HQ}. The other syringe was loaded with 1 mM DT and 20 mM MgATP. As turnover occurred in the [$Fe^{red}(MgATP)_2$–MoFe] complex, the oxidation of the [4Fe-4S] cluster of the Fe protein was monitored by an increase in absorbance at 426 nm. Data were fit to a single-exponential curve.

Quench-Flow Studies for ATP Hydrolysis

Pre-steady-state ATP hydrolysis experiments were performed using a rapid chemical quench flow (KinTek) in a Coy chamber (Grass Lake, MI) under a argon atmosphere. Mixtures were prepared in 50 mM MOPS (pH 7.4). Syringe A contained 80 μM Fe and 20 μM MoFe

proteins with either 10 mM DT or a 500 μM Fld^{HQ}/10 mM DT mixture. Syringe B contained 6 mM ATP and 8 mM $MgCl_2$ with [α-^{32}P]ATP. Eighteen microliters from syringe A was mixed with 18 μL from syringe B and then the reaction rapidly quenched with 45 μL of 0.75 M formic acid contained in syringe C. Aliquots (1 μL) of the quenched mixture were plated on TLC plates, and the ratios of [α-^{32}P]ATP to [α-^{32}P]ADP formed were analyzed as described above for the steady-state ATP hydrolysis experiments.

Real-Time Measurement of Inorganic Phosphate (P_i) Release

P_i release was assessed in a stopped-flow (SF) fluorometer (Auto SF-120, KinTek Corp.) using a coumarin {*N*-[2-(1-maleimidyl)ethyl]-7-(diethylamino) coumarin-3-carboxamide}-labeled phosphate binding protein (MDCC-PBP) assay.[43] P_i was quantified from binding MDCC-PBP that was monitored by an increase in fluorescence (λ_{exc} = 430 nm; λ_{em} > 450 nm), using a standard curve generated with KH_2PO_4 as described previously.[43] The experiments were conducted at 25 °C in 25 mM HEPES (pH 7.4) containing 1 mM DT. The SF syringes and flow lines were treated with a P_i mop [25 mM HEPES buffer (pH 7.4) with 320 μM 7-methylguanine (7-meG), and 0.12 unit/mL purine nucleoside phosphorylase (PNPase)] before each experiment for 45 min to remove contaminating P_i and then rinsed with DT-reduced buffer. The same concentration of the P_i mop system was also added to the reaction mixtures. MoFe (1 μM) and Fe (16 μM) were rapidly mixed with a solution of 25 μM MDCC-PBP, 7.5 mM $MgCl_2$, and 6 mM ATP, and the change in fluorescence was monitored over time; 100 μM Fld^{HQ} was added to the MoFe/Fe protein mixture to monitor the effect of Fld^{HQ} on P_i release.

In Silico Docking Study of Protein–Protein Interactions

In silico protein–protein docking simulations were performed using the computational docking program ClusPro 2.0. ClusPro 2.0 uses PIPER, a fast Fourier transform-based protein docking program with pairwise potentials, to derive the structure model. Flavodoxin II [Protein Data Bank (PDB) entry 1YOB] was used as the ligand and Fe protein (PDB entry 1FP6) as the receptor. The final docking model was chosen on the basis of the agreement of the electrostatic potentials of the bound complex, which were generated with PyMOL.

Biochemistry, Vol 55, No. 26 (July 5, 2016): pg. 3625-3635. DOI.

Time-Resolved Proteolysis of Flavodoxin and Fe Proteins

Limited proteolysis experiments were performed on Fe protein, Fld, and the Fe protein–Fld complex. Protein ratios of 1:1, 1:2, and 2:1 (Fe protein:Fld) were digested with Trypsin Gold (Promega, Madison, WI). The reactions were performed in sealed vials in a 50 mM ammonium bicarbonate, pH 8 buffer with1 mM sodium dithionite in a total volume of 120 μL and a protease:protein ratio of 1:1000 (w/w) at room temperature. Samples (15 μL) were taken at 0, 5, 10, 20, 40, 60, and 240 min. Reactions were quenched with 1 μL of 10% formic acid. Ten microliters of each sample was used for analysis of the trypsin digestion pattern by SDS–PAGE using a 4 to 20% linear gradient gel (Mini-Protean TGX, Bio-Rad, Hercules, CA).

Mapping of Proteolytic Cleavage Sites

The molecular weight of released peptides was determined using an Autoflex III MALDI-TOF/TOF mass spectrometer (Bruker Daltonics, Billerica, MA). One microliter of each sample was cocrystallized with a saturated solution of α-cyano-4-hydroxycinnamic acid matrix in 50% acetonitrile (Thermo-Fisher Scientific, Waltham, MA) containing 0.1% formic acid. Peptide mass spectra were acquired in positive reflectron mode with an acceleration voltage of 20 kV. Spectra were accumulations of 1000 laser shots. Spectra were averaged from three spots for each time point. Tryptic peptides were mapped to the protein sequence using the Protein Analysis Worksheet (PAWS) software package (ProteoMetrics, LLC). Results were mapped onto the ClusPro 2.0 Docking model.

Chemical Cross-Linking

Chemical cross-linking experiments were performed with Fe protein (20 μM) and Fld (Fe protein:Fld ratios of 2:1, 1:1, and 1:2) using 10 mM glutaraldehyde in 50 mM HEPES (pH 7.5), 150 mM NaCl, and 1 mM sodium dithionite. Reaction conditions were optimized to limit formation of higher-order aggregates. Samples were incubated with glutaraldehyde for 10 min, at room temperature. The reaction was quenched with 100 mM Tris buffer (pH 8.0). To preserve the native state and conformation of proteins and proteins in complex with their cofactors, all steps were performed under strict anaerobic

Biochemistry, Vol 55, No. 26 (July 5, 2016): pg. 3625-3635. DOI.

conditions. Complex formation and cross-linking were initiated at the same time.

Cross-linked samples and controls were analyzed by SDS–PAGE (4 to 20% linear gradient Mini-Protean TGX, Bio-Rad). Protein bands corresponding to monomers and dimers were digested with trypsin as previously described[44] prior to mass spectrometry analysis. LC–MS/MS measurements were performed using a maXis Impact UHR-QTOF instrument (Bruker Daltonics) interfaced with an Agilent 1100 HPLC nanoflow system (Agilent Technologies, Santa Clara, CA). Peptide mixtures were separated on a Dionex column (20 mm × 100 μm, 5 μm, 100 Å, Acclaim PepMap100, C18, Dionex), kept at 40 °C, and eluted with a flow rate of 800 nL/min in solvents A (0.1% formic acid) and B (acetonitrile/0.1% formic acid) with the following gradient: 3 to 30% B over 16 min, followed by 30 to 95% B over 3 min and a 5 min 95% B column wash step. The column was equilibrated with 3% B for 2 min prior to the next injection. Electrospray conditions in both MS and auto MS/MS modes were as follows: drying gas flow of 4.0 L/min at 100 °C, capillary voltage of 1600 V. Data were collected over the *m*/*z* range of 300–1700 at an acquisition rate of two spectra per second for MS and MS/MS. A linear voltage gradient depending on the mass:charge ratio was applied for peptides fragmented in auto MS/MS experiments with a decreasing order of preference +2 > +3 > +4 > +1 charged parent ions. Raw data were converted to mgf format using MS Convert and uploaded to SearchGUI (version 1.26.6.) for sequence identification and visualized and validated in PeptideShaker (version 0.40.1).[45] Validated peptides with an identification confidence higher than 95% were selected for further analysis.

Results and Discussion

Establishing k_{cat} with DT or Fld^{HQ}

In the two-component catalytic system of nitrogenase, both the Fe protein and the MoFe protein are catalysts. The rate-limiting step for the overall reaction is held to be the dissociation step in the Fe protein cycle (Figure 2). This means that the rate constant of the rate-limiting step should be the same as the k_{cat} for both Fe protein and MoFe protein cycles in terms of the number of electrons donated or accepted per active site per unit time. Earlier studies established a turnover number (k_{cat}) for electron flow to substrate reduction of

Biochemistry, Vol 55, No. 26 (July 5, 2016): pg. 3625-3635. DOI.

between 5 and 10 s^{-1} regardless of substrate.[31, 46] This value is approximately the same as the first-order rate constant for dissociation of $Fe^{ox}(MgADP)_2$ from the MoFe protein of ~6 s^{-1}, leading to the conclusion that the overall reaction rate-limiting step is dissociation (Figure 2).[1, 16-18, 31] However, a few previous studies have shown that the rate of dissociation of the Fe–MoFe protein complex using DT is slower than the k_{cat} under saturating ("high-flux") conditions.[40, 46]

Here, we determined the V_{max} values for both Fe protein and MoFe protein cycles using either DT or Fld as a reductant by varying the ratio of Fe protein to MoFe protein (called the "electron flux"). The V_{max} values for the Fe protein cycle were determined under low-flux conditions with a molar ratio of 1:1 ([Fe]:[MoFe]) for acetylene reduction and 1:2 for proton reduction using either DT or a Fld^{HQ}/DT mixture as a reductant. These "low-flux" conditions saturated the Fe protein with MoFe protein and resulted in a Fe protein cycle $k_{cat,Fe}$ of ~6 s^{-1} with DT as a reductant. When a Fld^{HQ}/DT mixture was used as the reductant, a $k_{cat,Fe}$ of 10–11 s^{-1} was observed (Table 1 and section S1 and Figures S1–S4). These results reveal that using Fld as a reductant accelerates the overall reaction, suggesting that the rate-limiting dissociation step has been accelerated by ~2-fold when Fld is the reductant compared to the dissociation rate constant when DT is the reductant.[40] This enhancement of V_{max} and k_{cat} of both Fe and MoFe protein is dependent on the electron flux, with a lower flux showing the largest effect (Figures S2–S5). When the electron flux is increased to saturate the MoFe protein with Fe protein ("high flux", 16–20:1 [Fe]:[MoFe]) to measure the MoFe protein cycle, the k_{cat} is found to be ~10–11 s^{-1} with both DT and Fld as the reductant. The increase in $k_{cat,Fe}$ observed for Fld^{HQ} compared to that with DT as the reductant could be explained by an increase in the rate of dissociation of the Fe protein from the MoFe protein when Fld^{HQ} is the reductant under low-flux conditions. To test this, we determined an apparent dissociation rate constant for the $Fe^{ox}(ADP)_2$–MoFe protein complex with either DT or Fld as the reductant.

Table 1. Steady-State k_{cat} Values for Fe Protein and MoFe Protein with Different Reductants

Biochemistry, Vol 55, No. 26 (July 5, 2016): pg. 3625-3635. DOI.

protein	reductant	k_{cat} (s^{-1})[a]
Fe protein	DT	5–6
	Fld^{HQ}	10–11
MoFe protein	DT	10–11
	Fld^{HQ}	10–11

a

The steady-state k_{cat} values for Fe protein and MoFe protein were estimated on the basis of the V_{max} of Fe protein (MW ≈ 64000 Da) under low-electron flux conditions and V_{max} of MoFe protein (MW ≈ 240000 Da) under high-flux conditions. For detailed reaction conditions, refer to the legends for Figures S1–S4 and Table S1.

Dissociation of $Fe^{ox}(ADP)_2$ from the MoFe Protein

To determine the apparent dissociation constant using SF spectrophotometry, the $Fe^{ox}(ADP)_2$–MoFe protein complex was preformed in one syringe of the SF spectrophotometer and rapidly mixed against a reductant mixture. Here, such experiments were conducted with either DT or Fld^{HQ} in the second syringe. The reduction of the Fe^{ox} was monitored at 426 nm, an isosbestic point for reversible conversion between Fld^{SQ} and Fld^{HQ} (Figure S6). As shown in Figure 3, the estimated first-order rate constant for dissociation (k_{obs}) with DT as a reductant was ~4 s^{-1}. When Fld^{HQ} was the reductant, the dissociation and reduction of $Fe^{ox}(ADP)_2$ were much more rapid, with a

Biochemistry, Vol 55, No. 26 (July 5, 2016): pg. 3625-3635. DOI.

majority of the reduction (~65%) occurring in <1 ms. A k_{obs} of >760 s^{-1} was estimated from a fit of the points captured after the dead time. These findings reveal that with Fld^{HQ} as the reductant, the reduction of Fe^{ox} is much faster than the observed k_{cat}, implying that dissociation of $Fe^{ox}(ADP)_2$ from the MoFe protein is not the rate-limiting step when Fld^{HQ} is used as the reductant. These results are consistent with the previously reported data from similar experiments.[25] To further test the effect of the reductant on the apparent rate of dissociation, another nonphysiological reductant, methyl viologen, was tested.[47] As can be seen in Figure 3, this electron donor gave a k_{obs} of 100 s^{-1}, again much faster than the k_{cat}.

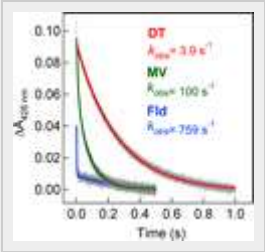

Figure 3. Reduction of $Fe^{ox}(ADP)_2$ protein by DT (red), MV (green), or Fld^{HQ} (blue) in the presence of MoFe protein. The reduction of $Fe^{ox}(ADP)_2$ by different reductants was monitored as the decrease in the absorbance at 426 nm as a function of time. The data are displayed as gray dots and were fit to different equations as described in Materials and Methods to obtain the pseudo-first-order k_{obs}. Syringe 1 contained 20 mM DT with 100 μM MV or 400 μM Fld^{HQ} with 20 mM DT. Syringe 2 contained 80 μM Fe^{ox} and 80 μM MoFe. MgADP (9 mM) was present in both syringes.

The faster reduction of $Fe^{ox}(ADP)_2$ in the presence of MoFe protein by Fld^{HQ} could be explained by two possible mechanisms: (i) the very rapid dissociation of $Fe^{ox}(ADP)_2$ from the MoFe protein when Fld^{HQ} is the reductant, pointing to a different rate-limiting step,[40] or (ii) Fld^{HQ} reduction of the Fe protein while it is still complexed to the MoFe protein,[48] a mechanism proposed earlier by Haaker et al.[25] To test the second model, the ability of Fld^{HQ} to reduce $Fe^{ox}(ADP)_2$ while still bound to the MoFe protein was examined.

Effect of Fld^{HQ} on the Primary Electron Transfer of Nitrogenase

Biochemistry, Vol 55, No. 26 (July 5, 2016): pg. 3625-3635. DOI.

The pre-steady-state ET from the Fe protein to the MoFe protein offers a straightforward way to monitor the possibility of ET from Fld^{HQ} to Fe^{ox} while it is still bound to the MoFe protein. When the Fe^{red}–MoFe protein mixture is mixed with MgATP in a SF spectrophotometer, an apparent first-order ET event is monitored by the increase in absorbance (oxidation of the Fe protein) that can be fit to a single exponential to yield a rate constant for ET (k_{ET}). With DT as the reductant, a k_{ET} of 173 s^{-1} was observed (Figure 4), consistent with literature values that range from 140 to 200 s^{-1}.[14-16, 22, 25] Importantly for this study, the absorbance value plateaus starting at 10 ms and stays roughly flat up to 30 ms. This plateau in absorbance reflects no reduction by DT of the Fe^{ox} protein while it is still in the complex. At much later times (100 ms), the absorbance does change, reflecting a complex set of events as the Fe protein dissociates from the MoFe protein, is reduced, and rebinds to the MoFe protein. When the ET study is conducted with Fld^{HQ} as the reductant, nearly identical primary ET kinetics are observed (Figure 4). Importantly, no reduction of the Fe^{ox} protein is observed during the 10–30 ms time frame. Given the earlier observation of the rate of reduction of the $Fe^{ox}(ADP)_2$ protein–MoFe protein complex with Fld^{HQ} being >760 s^{-1}, an on-complex reduction of the Fe protein in the ET study should have resulted in a significant (if not complete) reduction of the Fe protein before 10 ms. The lack of any observed reduction of the Fe^{ox} protein in the ET experiment reveals that the Fld^{HQ} protein reduction of the $Fe^{ox}(ADP)_2$ protein in a complex with the MoFe protein must be very slow, as reported previously.[48] Thus, these studies, coupled with the dissociation studies presented in the previous section, rule out Fld^{HQ} reduction of the Fe protein while it is still bound to the MoFe protein[25] and instead favor a rapid dissociation of $Fe^{ox}(ADP)_2$ protein from the MoFe protein when Fld^{HQ} is the reductant.

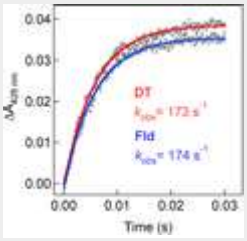

Figure 4. Primary ET from $Fe^{red}(ATP)_2$ protein to MoFe protein in the presence of DT or Fld^{HQ} with DT. Syringe 1 contained 80 μM Fe^{red}

Biochemistry, Vol 55, No. 26 (July 5, 2016): pg. 3625-3635. DOI.

protein, 20 μM MoFe protein, 1 mM DT, and 10 mM MgATP. Syringe 2 contained 10 mM DT or 200 μM Fld^{HQ} with 1 mM DT in the presence of 10 mM MgATP.

Reduction of Fe^{ox} Protein by DT and Fld^{HQ}

The studies, to this point, favor rapid dissociation of the $Fe^{ox}(ADP)_2$ protein from the MoFe protein when Fld^{HQ} is the reductant. The observed lower rate of dissociation when DT is the reductant could indicate slow reduction of Fe^{ox} protein, rather than slow dissociation of the Fe protein from the MoFe protein.[17, 23, 25] Several previous studies have illustrated low activity for nitrogenase at low a concentration of $SO_2^{\bullet-}$ as the reductant.[17-19, 22, 49] To determine the rates of reduction of Fe^{ox} protein by different reductants, the pre-steady-state studies were conducted using Fe^{ox} in the absence and presence of a nucleotide (ADP or ATP). Fe^{ox} protein in one syringe was rapidly mixed against either DT or Fld^{HQ} in the other syringe. Additionally, these studies were conducted at 4 °C to slow the reactions enough to observe them. Consistent with previous studies, nucleotides significantly slow the rates of reduction of Fe^{ox} protein by DT (by ~100-fold).[22, 23] In contrast, with Fld^{HQ} as the reductant, the rates of reduction remained fast and roughly unchanged with or without nucleotide present (Figure 5).[25, 27]

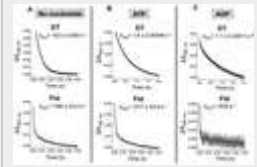

Figure 5. Kinetics of the reduction of Fe^{ox} protein by DT and Fld^{HQ} with DT in the presence and absence of nucleotides. ET is monitored by observing the change in absorbance at 426 nm as a function of time. (A) Reduction of Fe protein by DT and Fld^{HQ} with DT with no nucleotide. (B) Reduction of Fe protein by DT and Fld^{HQ} with DT in the presence of MgADP. (C) Reduction of Fe protein by DT and Fld^{HQ} with DT in the presence of MgATP. Syringe 1 contained 80 μM Fe^{ox}. Syringe 2 contained 20 mM DT or 600 μM Fld^{HQ} with 20 mM DT. MgADP and MgATP, when included, were present in both syringes at a final concentration of 10 mM. The k_{obs} values were averaged from two independent experiments except for that of Fld with MgATP.

Biochemistry, Vol 55, No. 26 (July 5, 2016): pg. 3625-3635. DOI.

Taken together, the studies presented so far suggest that when Fld^{HQ} is the reductant, dissociation of $Fe^{ox}(ADP)_2$ from the MoFe protein is not rate-limiting and does not correspond to the overall k_{cat} for substrate reduction. Rather, the dissociation step when Fld^{HQ} is used as the reductant is much more rapid than the k_{cat}.

Protein–Protein Interaction between the Fe Protein and Fld

The results presented so far indicate that Fld^{HQ} does not reduce the Fe protein while it is still complexed to the MoFe protein, suggesting that reduction occurs only after the Fe protein is free from the MoFe protein. We next employed molecular modeling to predict where the Fld would bind to the Fe protein to achieve ET. The docking model produced by ClusPro 2.0 predicts the binding of one Fld monomer to a dimer of Fe protein (Figure 6A). The distance between the [4Fe-4S] cluster at the active site of the Fe protein and the FMN of the Fld measured in PyMOL was within electron transfer distance (<10 Å) (Figure 6B).

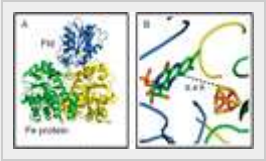

Figure 6. Interaction of Fe protein and Fld for ET. (A) The docking model from ClusPro 2.0 predicts the binding of one Fld monomer to a dimer of Fe protein. The complex structure shows the nitrogenase Fe protein with subunits colored yellow and green (PDB entry 1FP6), and Fld (NifF) is colored blue (PDB entry 1YOB). (B) Close-up of the docked proteins. The distance between the [4Fe-4S] cluster at the active site of the iron protein and the FMN cofactor at the active site of the flavodoxin is predicted to be 6.4 Å.

Analysis of electrostatic potentials performed in PyMOL demonstrated qualitative agreement with the ClusPro 2.0 docking model. The highly negative patch at the FMN cofactor of Fld sits on top of the highly positive patch at the location of the [4Fe-4S] cluster of the Fe protein (Figure S7). Salt bridge interactions were identified in the proposed complex binding region on either side of the FMN cofactor of Fld and the [4Fe-4S] cluster of the Fe protein (Figure 7A). The identified residues are Arg100 on one of the Fe protein subunits

Biochemistry, Vol 55, No. 26 (July 5, 2016): pg. 3625-3635. DOI.

and Glu104 of Fld and Arg140 of the Fe protein and Asp154 of Fld. These salt bridge interactions further support the analysis that showed that electrostatic interactions between the Fe protein and Fld allow complex formation. Interestingly, the Fe protein Arg100 residue is the site of ADP ribosylation, which controls association of the Fe protein with the MoFe protein in response to the N status of the cell.[50, 51]

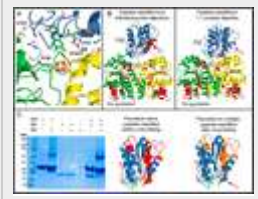

Figure 7. Mapping of the Fe protein–Fld interaction site. (A) Salt bridge interactions were identified in the proposed binding region on either side of the FMN cofactor of Fld (blue) and the [4Fe-4S] cluster of the Fe protein (FeP) (green and yellow). The identified residues were Arg100 on one of the Fe protein subunits (green) and Glu104 of flavodoxin and Arg140 on the other Fe protein subunit (yellow) and Asp154 of Fld. (B) Time-resolved proteolysis experiments show changes in Fld upon its binding to Fe protein. Fe protein and Fld were digested with trypsin before (B, left) and after formation of a complex (B, right). Mapping of the kinetically favored sites of cleavage revealed different patterns. One of the favored sites on Fld, which mapped near the binding surface with Fe protein (black arrow), was protected from cleavage in the complex (red arrow). (C) Addition of cross-linking reagent to the Fe protein–Fld complex [1:1 (w/w) protein ratio] resulted predominantly in formation of monomers (intraprotein linkages) and dimers (Fe protein–Fe protein and Fe protein–Fld interprotein linkages) (C, left). In addition to the cross-linked complex, the following controls were run: Fe protein, Fld, non-cross-linked Fe protein–Fld, and Fe protein and Fld cross-linked individually. To identify interacting domains, corresponding monomers and dimers were digested with trypsin and identified peptides (red) were mapped onto the ClusPro 2.0 Docking model (in panel C, middle and right panels show Fld and Fld in complex with Fe protein after exposure to glutaraldehyde, respectively). Fragments colored orange denote peptides underrepresented in the cross-linked sample with respect to unlabeled protein. The red arrow points to this part of the Fld structure that was absent after cross-linking.

Biochemistry, Vol 55, No. 26 (July 5, 2016): pg. 3625-3635. DOI.

Time-resolved limited proteolysis experiments were subsequently performed to test the docking model. These experiments involve incubation of proteins with proteases for varying lengths of time and then mapping the observed cleavages on the protein sequences. This approach facilitates identification of kinetically favored sites of protease cleavage. Via comparison of the peptide fragments before and after formation of a complex, regions that change conformation or are protected in the complex can be identified. Reactions were performed at Fe protein:Fld ratios of 1:1, 1:2, and, 2:1, and with the two proteins alone. Sites of proteolysis were identified using MALDI-TOF and LC–MS/MS and mapped onto the docking model. Cleavage sites on Fe protein were located on solvent-exposed surfaces under all conditions (Figure 7). Fewer sites were found on Fld; however, upon formation of the complex, Fld cleavage sites directly adjacent to the proposed binding surfaces (Figure 7B) were protected. Specifically, Fld tryptic fragment Lys15–Lys22 was no longer present when it was bound to Fe protein (Figure 7B). Furthermore, regions near the [4Fe-4S] cluster of the Fe protein and the FMN cofactor of Fld were not observed, indicating that these regions were also protected from proteolysis (Figure 7B). The proteolysis data are consistent with the docking model with respect to the surfaces involved in mediating protein–protein interactions.

While implied by our data and previous models, the stoichiometry of the solution phase complex has not been directly addressed. To investigate this, chemical cross-linking experiments were performed. Fe protein alone, Fld alone, and Fld after complex formation were covalently cross-linked using 20 mM glutaraldehyde (GA). The proteins were exposed to GA for 10 min before the reaction was quenched. Analysis of the samples by SDS–PAGE showed that the predominant species present was consistent with an Fe protein–Fld binary complex (Figure 7C, left). Mass spectrometry analysis confirmed the presence of both proteins in the gel band of interest. However, some peptide fragments were no longer detectable or were present in much smaller quantities when Fe protein and Fld were engaged in a complex and exposed to GA (Figure 7). For example, on the basis of Fld (Figure 7C, middle and left), there are three distinguished regions. (1) Colored in red, this part of the protein chain was easily digested by trypsin and was identified by LC–MS/MS with a high degree of confidence. One of the fragments, Ile125–Lys146, was

Biochemistry, Vol 55, No. 26 (July 5, 2016): pg. 3625-3635. DOI.

always detectable regardless of GA treatment, suggesting a lack of involvement in any kind of interactions (within Fld itself and/or between Fld and Fe protein). (2) Colored orange, these parts of the protein sequence were also identified; however, they were found in significantly lower concentrations in cross-linked samples, which implies more structured regions (within Fld itself) that were in the proximity and were linked with GA and/or protein sections potentially engaged in interactions with Fe protein; colored blue, this part of the Fld chain was not detected in any sample. Taken together, our observations from chemical labeling shows that Fld peptide fragment Phe147–Lys160 is directly involved in contact with Fe protein; however, more parts of the Fld sequence might be involved in complex formation through subtle adjustments to conformation.

The results from the *in silico* modeling, proteolysis, and cross-linking experiments all support the predicted 1:1 stoichiometry for the Fe protein–Fld interaction with an interface bringing the two cofactors ([4Fe-4S] cluster and FMN) close together to favor the ET (Figures 6 and 7 and Figure S7). The site of interaction with Fld on the Fe protein surface is the same as that in the MoFe protein. To test this prediction, we performed the proton reduction assay under both low- and high-electron flux conditions. The results display a significant inhibitory effect of Fld on the proton reduction activity (Figure S8) in the presence of 2.4 mM Fld^{HQ}, compared to those in the presence of 600 μM Fld^{HQ} (Figure S1). The observed inhibition from Fld further supports the transient interaction between the Fe protein and Fld during nitrogenase catalysis.[27]

Efficiency of ATP Hydrolysis per Electron Transferred for Substrate Reduction

It has been reported that Fld^{HQ} can reduce the Fe^{ox} protein by one electron to the $[4Fe\text{-}4S]^{+}$ state[25, 27] or by two electrons to the all ferrous $[4Fe\text{-}4S]^{0}$ state.[33, 34] From the all ferrous state, the Fe protein could deliver two electrons to the MoFe protein per association, resulting in two ATP molecules hydrolyzed per two electrons transferred.[33, 34, 40] This possibility is contrary to the consensus that each association event results in two ATP molecules hydrolyzed per electron transferred. Using DT as the reductant, the ATP:e^{-} ratio was found to be ~2:1 with three different substrates under high- or low-electron flux conditions (Table 2 and Figure S9). This result is

Biochemistry, Vol 55, No. 26 (July 5, 2016): pg. 3625-3635. DOI.

consistent with the previously reported data. Using Fld^{HQ} as the reductant, the ATP:e^- ratio was also found to be ~2:1 under high and low electron flux with three substrates. The results clearly indicate that approximately two ATP molecules were hydrolyzed per electron transferred [2:1 ATP:e^- (Table 2)], which was independent of substrate, reductant (DT or Fld^{HQ}), and electron flux condition. These findings are consistent with a single ET per association event coupled to the hydrolysis of two ATP molecules even when Fld^{HQ} is the reductant.[1, 52]

Table 2. Numbers of ATP Molecules Hydrolyzed per Electron Transferred for Reduction of Different Substrates by Nitrogenase under Different Electron Flux Conditions

		ATP:e^- ratio[d]		
reaction conditions[a]	**reductant**	**proton (Ar)**	**N_2 (1 atm)[e]**	**acetylene[f] (0.11 atm)**
low flux[b]	DT	1.87 ± 0.04	1.85	2.17 ± 0.07
	Fld^{HQ}	1.91 ± 0.05	1.91	2.26 ± 0.12
high flux[c]	DT	1.63 ± 0.12	1.82	1.89 ± 0.10
	Fld^{HQ}	1.96 ± 0.17	1.78	2.74 ± 0.21

a

Biochemistry, Vol 55, No. 26 (July 5, 2016): pg. 3625-3635. DOI.

All assays for product quantification were conducted in a buffer containing 8.5 mM MgATP without a regeneration system with 12 mM DT or 712 μM Fld^{HQ} and 10 mM DT. For ADP quantification assays, a trace concentration of [α-^{32}P]ATP was added to the reaction mixtures.

b
Low-flux assays were conducted using 1.95 μM Fe protein with 2.08 μM MoFe protein for proton and acetylene reduction and 4.16 μM MoFe protein for N_2 reduction.

c
High-flux assays were conducted with 0.41 μM MoFe protein and 8 μM Fe protein.

d
The ATP:e^- ratios for proton and acetylene reduction assays were averaged from the data at three different reaction times (Figure S1) with the standard deviation shown. N_2 reduction values were calculated from assays with a reaction time of 60 s.

e
Total electrons for H_2 and NH_3 production were counted.

f
Only electrons for ethylene production were counted as proton reduction was below the detection limit.

Pre-Steady-State and Steady-State Analysis of ATP Hydrolysis

On the basis of the findings presented to this point, we conclude that the Fe protein–MoFe protein dissociation step is not rate-limiting. What then is the rate-limiting step in the overall reaction cycle? In the Fe protein cycle using DT as the reductant (Figure 2), the ATP hydrolysis (k_{ATP} = 50–70 s^{-1}) and P_i release (k_{Pi} = 16–22 s^{-1}) steps both are slower than the ET (k_{ET} = 140–200 s^{-1}).

Comparing rate constants for ATP hydrolysis from pre-steady-state studies with DT or Fld^{HQ} as the reductant and a 1:4 ([MoFe]:[Fe])

electron flux revealed similar values ($k_{ATP,DT}$ and $k_{ATP,Fld}$) of 40 and 44 s^{-1} (25 °C), respectively (Figure 8). These rate constants are approximately double the k_{cat} (10–11 s^{-1}) when considering that two ATP molecules are hydrolyzed per electron, indicating that ATP hydrolysis is not the rate-limiting step for the overall reaction. The steady-state (linear) rates of ATP hydrolysis are found to be $k_{ATP,DT}$ = 10 s^{-1} and $k_{ATP,Fld}$ = 20 s^{-1} (25 °C), consistent with the k_{cat} values reported here. The slow steady-state ATP hydrolysis rate using DT matches the slow reduction rate of $Fe^{ox}(ADP)_2$ and $Fe^{ox}(ATP)_2$ (k_{obs} = 5–6 s^{-1}) by DT, whereas the faster $k_{ATP,Fld}$ is consistent with the faster reduction of the $Fe^{ox}(ADP)_2$ and $Fe^{ox}(ATP)_2$ states by Fld^{HQ} (Figure 5).[22, 23] The ATP hydrolysis rate constant obtained under high-flux conditions ([MoFe]:[Fe] = 1:16) showed no difference in the pre-steady-state rate constants for ATP hydrolysis with DT or Fld as the reductant (data not shown). However, the steady-state rate constant for ATP hydrolysis using DT is significantly increased to 25 s^{-1}, which is approximately the same as the value when using Fld^{HQ} (27 s^{-1}) under the same conditions. It is interesting that the steady-state ATP hydrolysis rate constant (25–27 s^{-1}) is approximately the same as those previously reported for the pre-steady-state P_i release step [16–22 s^{-1} (Figure 2)].[16, 18] Given that two P_i molecules are released per electron transferred, the P_i release rate constant should be double the k_{cat} value (~20 s^{-1}) if this step is the overall rate-limiting step.

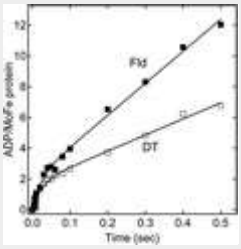

Figure 8. Time course of pre-steady-state and steady-state ATP hydrolysis during nitrogenase catalysis under Ar with DT (□) or Fld^{HQ} with DT (■) as the reductant at 25 °C. The hydrolysis of ATP was monitored with [α-^{32}P]ATP as a tracing reagent. The ADP:MoFe protein ratio was plotted as a function of time. The data were fitted to two phases: a burst exponential followed by a linear steady state for both DT and Fld^{HQ} with DT. The pre-steady-state burst phase gave first-order rate constants: $k_{ATP,DT}$ = 40 s^{-1}, and $k_{ATP,Fld}$ = 44 s^{-1}. The steady-

Biochemistry, Vol 55, No. 26 (July 5, 2016): pg. 3625-3635. DOI.

state linear phase gave the following rate constants: $k_{ATP,DT}$ = 10 s^{-1}, and $k_{ATP,Fld}$ = 20 s^{-1}.

P_i Release Events

P_i release was measured using an established fluorometric method[43] with either DT or Fld^{HQ} as the reductant under high-electron flux conditions (16:1 [Fe]:[MoFe]). The data showed an initial lag phase followed by a linear phase with both reductants, with the linear phases having the following rate constants for P_i release: $k_{Pi,DT}$ = 27 s^{-1}, and $k_{Pi,Fld}$ = 25 s^{-1} (Figure 9). These rate constants are approximately double the overall reaction rate constant k_{cat} of 10–11 s^{-1} per electron. Two P_i molecules are released for each electron transferred, showing that the overall rate-limiting step is likely an event associated with P_i release. We have no data on the ADP release event, so the position of this event in the cycle remains unknown.

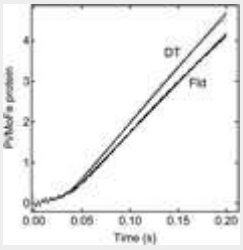

Figure 9. P_i release. Real-time measurement of P_i release during nitrogenase catalysis using DT (gray) or Fld^{HQ} with DT (black) as the reductant at 25 °C. P_i release was monitored by a fluorescence increase caused by the binding of P_i to MDCC-PBP. The P_i:MoFe protein ratio is plotted as a function of time. After the initial lag phase (~30 ms), the data collected from 40 to 200 ms were fitted to a linear equation (—), giving the following rate constants: $k_{Pi,DT}$ = 27 s^{-1}, and $k_{Pi,Fld}$ = 25 s^{-1}.

Establishing the Rate-Limiting Step in the Fe Protein Cycle

Considering all of the rate constants for the steps in the Fe protein cycle with Fld^{HQ} as the reductant [electron transfer (k_{ET} = 173 s^{-1}), ATP hydrolysis (k_{ATP} ~ 40–44 s^{-1}), P_i release (25–27 s^{-1}), and re-reduction of $Fe^{ox}(ADP)_2$ (k_{obs} > 1200 s^{-1})], we conclude that the overall rate-limiting steps for the reaction are events associated with the P_i

release step, not complex dissociation. Our findings are consistent with those presented for other ATP-hydrolyzing systems, including helicases[53, 54] and myofibrillar ATPases,[55-58] where P_i release is the rate-limiting step.

Summary

The Fe protein cycle can now be updated with the rate constants determined here using Fld^{HQ} as the reductant, as shown in Figure 10. The cycle begins with the rapid equilibrium docking of $Fe^{red}(ATP)_2$ to MoFe protein, which is followed by the conformationally gated ET events. The next step is ATP hydrolysis, which is followed by events associated with P_i release. It is unknown if the P_i release event is conformationally gated, but it is clear that events associated with this step are rate-limiting for the overall Fe protein cycle. The dissociation of $Fe^{ox}(ADP)_2$ is fast, with rapid reduction by Fld^{HQ}. Finally, ATP replaces ADP in the free Fe protein. The order of these last two events is not established, but the rapid reduction by Fld^{HQ} suggests that reduction should occur before nucleotide exchange.

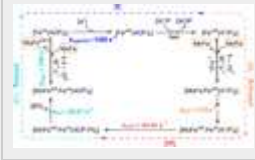

Figure 10. Updated Fe protein cycle with Fld^{HQ} as the reductant.

Supporting Information

The Supporting Information is available free of charge on the ACS Publications website at DOI: 10.1021/acs.biochem.6b00421.

- Electron distribution for H_2 and NH_3 production (Table S1), acetylene reduction by wild-type Mo-nitrogenase (Figure S1), dependence of electron flux on proton reduction (Figure S2), dependence of electron flux on N_2 reduction (Figure S3), dependence of electron flux on the total activity of proton and N_2 reduction under N_2 (Figure S4), dependence of electron flux on MoFe protein activity for N_2 reduction (Figure S5), isosbestic point in UV–vis spectra for conversion of Fld^{HQ} to Fld^{SQ} (Figure S6),

Biochemistry, Vol 55, No. 26 (July 5, 2016): pg. 3625-3635. DOI.

electrostatic analysis of Fld–Fe protein interaction (Figure S7), inhibition of nitrogenase activity by a high concentration of Fld (Figure S8), and time course of ATP hydrolysis and electron utilization (Figure S9) (PDF)

- **PDF**
  - bi6b00421_si_001.pdf (875.29 kB)

Evidence That the P_i Release Event Is the Rate-Limiting Step in the Nitrogenase Catalytic Cycle

fig**share**

ShareDownload

Funding Information
This work was supported as part of the Biological Electron Transfer and Catalysis Energy Frontier Research Center funded by the U.S. Department of Energy, Office of Science, Basic Energy Sciences, via Grant DE-SC0012518.

The authors declare no competing financial interest.

Acknowledgment

The authors thank the members of the Biological Electron Transfer and Catalysis Energy Frontiers Research Center for helpful discussions.

Abbreviations

ET	electron transfer
Fe^{red}	reduced Fe protein
Fe^{ox}	oxidized Fe protein

DT	dithionite
Fld	flavodoxin
Fd	ferredoxin
Fld^{Q}	oxidized flavodoxin quinone
Fld^{SQ}	one-electron-reduced flavodoxin semiquinone
Fld^{HQ}	reduced flavodoxin hydroquinone
IPTG	isopropyl β-D-1-thiogalactopyranoside
SF	stopped-flow
PMS	phenazine methosulfate
GA	glutaraldehyde.

References

This article references 58 other publications.

[1]Burgess, B. K. and Lowe, D. J. (**1996**) Mechanism of molybdenum nitrogenase *Chem. Rev.* 96, 2983– 3012, DOI: 10.1021/cr950055x

[2]Seefeldt, L. C., Hoffman, B. M., and Dean, D. R. (**2009**) Mechanism of Mo-dependent nitrogenase *Annu. Rev. Biochem.* 78, 701– 722, DOI: 10.1146/annurev.biochem.78.070907.103812

[3]Hoffman, B. M., Lukoyanov, D., Yang, Z.-Y., Dean, D. R., and Seefeldt, L. C. (**2014**) Mechanism of nitrogen fixation by nitrogenase: the next stage *Chem. Rev.* 114, 4041– 4062, DOI: 10.1021/cr400641x

[4]Hageman, R. V. and Burris, R. H. (**1978**) Nitrogenase and nitrogenase reductase associate and dissociate with each catalytic cycle *Proc. Natl. Acad. Sci. U. S. A.* 75, 2699– 2702, DOI: 10.1073/pnas.75.6.2699

[5]Georgiadis, M. M., Komiya, H., Chakrabarti, P., Woo, D., Kornuc, J. J., and Rees, D. C. (**1992**) Crystallographic structure of the nitrogenase iron protein from *Azotobacter vinelandii Science* 257, 1653– 1659, DOI: 10.1126/science.1529353

[6]Seefeldt, L. C., Hoffman, B. M., and Dean, D. R. (**2012**) Electron transfer in nitrogenase catalysis *Curr. Opin. Chem. Biol.* 16, 19– 25, DOI: 10.1016/j.cbpa.2012.02.012

[7]Chan, M. K., Kim, J., and Rees, D. C. (**1993**) The nitrogenase FeMo-cofactor and P-cluster pair: 2.2 Å resolution structures *Science* 260, 792– 794, DOI: 10.1126/science.8484118

[8]Kim, J. and Rees, D. C. (**1992**) Structural models for the metal centers in the nitrogenase molybdenum-iron protein *Science* 257, 1677– 1682, DOI: 10.1126/science.1529354

[9]Einsle, O., Tezcan, F. A., Andrade, S. L. A., Schmid, B., Yoshida, M., Howard, J. B., and Rees, D. C. (**2002**) Nitrogenase MoFe-protein at 1.16 Å resolution: A central ligand in the FeMo-cofactor *Science* 297, 1696– 1700, DOI: 10.1126/science.1073877

[10]Spatzal, T., Aksoyoglu, M., Zhang, L., Andrade, S. L. A., Schleicher, E., Weber, S., Rees, D. C., and Einsle, O. (**2011**) Evidence for interstitial carbon in nitrogenase FeMo cofactor *Science* 334, 940– 940, DOI: 10.1126/science.1214025

[11]Lancaster, K. M., Roemelt, M., Ettenhuber, P., Hu, Y., Ribbe, M. W., Neese, F., Bergmann, U., and DeBeer, S. (**2011**) X-ray emission spectroscopy evidences a central carbon in the nitrogenase iron-molybdenum cofactor *Science* 334, 974– 977, DOI: 10.1126/science.1206445

[12]Thorneley, R. N., Lowe, D. J., Eday, R. R., and Miller, R. W. (**1979**) The coupling of electron transfer in nitrogenase to the hydrolysis of magnesium adenosine triphosphate *Biochem. Soc. Trans.* 7, 633– 636, DOI: 10.1042/bst0070633

[13]Hageman, R. V., Orme-Johnson, W. H., and Burris, R. H. (**1980**) Role of magnesium adenosine 5'-triphosphate in the hydrogen evolution reaction catalyzed by nitrogenase from *Azotobacter vinelandii Biochemistry* 19, 2333– 2342, DOI: 10.1021/bi00552a009

[14]Danyal, K., Dean, D. R., Hoffman, B. M., and Seefeldt, L. C. (**2011**) Electron transfer within nitrogenase: Evidence for a deficit-spending mechanism *Biochemistry* 50, 9255– 9263, DOI: 10.1021/bi201003a

[15]Danyal, K., Mayweather, D., Dean, D. R., Seefeldt, L. C., and Hoffman, B. M. (**2010**) Conformational gating of electron transfer from the nitrogenase Fe protein to MoFe protein *J. Am. Chem. Soc.* 132, 6894– 6895, DOI: 10.1021/ja101737f

[16]Duval, S., Danyal, K., Shaw, S., Lytle, A. K., Dean, D. R., Hoffman, B. M., Antony, E., and Seefeldt, L. C. (**2013**) Electron transfer precedes ATP hydrolysis during nitrogenase catalysis *Proc. Natl. Acad. Sci. U. S. A.* 110, 16414– 16419, DOI: 10.1073/pnas.1311218110

[17]Thorneley, R. N. F. and Lowe, D. J. (**1983**) Nitrogenase of *Klebsiella pneumoniae*. Kinetics of the dissociation of oxidized iron protein from molybdenum-iron protein: Identification of the rate-limiting step for substrate reduction *Biochem. J.* 215, 393– 403, DOI: 10.1042/bj2150393

[18]Wilson, P. E., Nyborg, A. C., and Watt, G. D. (**2001**) Duplication and extension of the Thorneley and Lowe kinetic model for *Klebsiella pneumoniae* nitrogenase catalysis using a MATHEMATICA software platform *Biophys. Chem.* 91, 281– 304, DOI: 10.1016/S0301-4622(01)00182-X

[19]Thorneley, R. N. F. and Lowe, D. J. (**1985**) Kinetics and mechanisms of the nitrogenase enzyme system. In *Molybdenum Enzymes* (Spiro, T. G., Ed.) pp 221– 284, Wiley, New York.

[20]Seefeldt, L. C., Yang, Z.-Y., Duval, S., and Dean, D. R. (**2013**) Nitrogenase reduction of carbon-containing compounds *Biochim. Biophys. Acta, Bioenerg.* 1827, 1102– 1111, DOI: 10.1016/j.bbabio.2013.04.003

[21]Lowe, D. J. and Thorneley, R. N. (**1984**) The mechanism of *Klebsiella pneumoniae* nitrogenase action: The determination of rate constants required for the simulation of the kinetics of N_2 reduction and H_2 evolution *Biochem. J.* 224, 895– 901, DOI: 10.1042/bj2240895

[22]Ashby, G. A. and Thorneley, R. N. F. (**1987**) Nitrogenase of *Klebsiella pneumoniae*: Kinetic studies on the Fe protein involving reduction by sodium dithionite, the binding of MgADP and a conformation change that alters the reactivity of the 4Fe-4S centre *Biochem. J.* 246, 455– 465, DOI: 10.1042/bj2460455

[23]Wilson, P. E., Bunker, J., Lowery, T. J., and Watt, G. D. (**2004**) Reduction of nitrogenase Fe protein from *Azotobacter vinelandii* by dithionite: Quantitative and qualitative effects of nucleotides, temperature, pH and reaction buffer *Biophys. Chem.* 109, 305– 324, DOI: 10.1016/j.bpc.2003.12.002

[24]Yates, M. G. (**1972**) Electron transport to nitrogenase in *Azotobacter chroococcum*: *Azotobacter* flavodoxin hydroquinone as an electron donor *FEBS Lett.* 27, 63– 67, DOI: 10.1016/0014-5793(72)80410-1

[25]Duyvis, M. G., Wassink, H., and Haaker, H. (**1998**) Nitrogenase of *Azotobacter vinelandii*: Kinetic analysis of the Fe protein redox cycle *Biochemistry* 37, 17345– 17354, DOI: 10.1021/bi981509y

[26]Bennett, L. T., Jacobson, M. R., and Dean, D. R. (**1988**) Isolation, sequencing, and mutagenesis of the *nif*F gene encoding flavodoxin from *Azotobacter vinelandii J. Biol. Chem.* 263, 1364– 1369

[27]Thorneley, R. N. and Deistung, J. (**1988**) Electron-transfer studies involving flavodoxin and a natural redox partner, the iron protein of nitrogenase: Conformational constraints on protein-protein interactions and the kinetics of electron transfer within the protein complex *Biochem. J.* 253, 587– 595, DOI: 10.1042/bj2530587

[28]Mortenson, L. E. (**1964**) Ferredoxin and ATP, requirements for nitrogen fixation in cell-free extracts of *Clostridium pasteurianum Proc. Natl. Acad. Sci. U. S. A.* 52, 272– 279, DOI: 10.1073/pnas.52.2.272

[29]Martin, A. E., Burgess, B. K., Iismaa, S. E., Smartt, C. T., Jacobson, M. R., and Dean, D. R. (**1989**) Construction and characterization of an *Azotobacter vinelandii* strain with mutations in the genes encoding flavodoxin and ferredoxin I *J. Bacteriol.* 171, 3162– 3167

[30]Saeki, K. (**2004**) Electron transport to nitrogenase: Diverse routes for a common destination. In *Genetics and regulation of nitrogen fixation in free-living bacteria* (Klipp, W., Masephol, B., Gallon, J. R., and Newton, W. E., Eds.) pp 257– 290, Kluwer Academic Publishers, Dordrecht, The Netherlands.

[31]Hageman, R. V. and Burris, R. H. (**1978**) Kinetic studies on electron transfer and interaction between nitrogenase components from *Azotobacter vinelandii Biochemistry* 17, 4117– 4124, DOI: 10.1021/bi00613a002

[32]Simpson, F. B. and Burris, R. H. (**1984**) A nitrogen pressure of 50 atm does not prevent evolution of hydrogen by nitrogenase *Science* 224, 1095– 1097, DOI: 10.1126/science.6585956

[33]Erickson, J. A., Nyborg, A. C., Johnson, J. L., Truscott, S. M., Gunn, A., Nordmeyer, F. R., and Watt, G. D. (**1999**) Enhanced efficiency of ATP hydrolysis during nitrogenase catalysis utilizing reductants that form the all-ferrous redox state of the Fe protein *Biochemistry* 38, 14279– 14285, DOI: 10.1021/bi991389+

[34]Lowery, T. J., Wilson, P. E., Zhang, B., Bunker, J., Harrison, R. G., Nyborg, A. C., Thiriot, D., and Watt, G. D. (**2006**) Flavodoxin hydroquinone reduces *Azotobacter vinelandii* Fe protein to the all-ferrous redox state with a S = 0 spin state *Proc. Natl. Acad. Sci. U. S. A.* 103, 17131– 17136, DOI: 10.1073/pnas.0603223103

[35]Fisher, K., Hare, N. D., and Newton, W. E. (**2014**) Another role for CO with nitrogenase? CO stimulates hydrogen evolution catalyzed by variant *Azotobacter vinelandii* Mo-Nitrogenases *Biochemistry* 53, 6151– 6160, DOI: 10.1021/bi500546k

[36]Benemann, J. R., Yoch, D. C., Valentine, R. C., and Arnon, D. I. (**1969**) The electron transport system in nitrogen fixation by *Azotobacter*, I: Azotoflavin as an electron carrier *Proc. Natl. Acad. Sci. U. S. A.* 64, 1079– 1086, DOI: 10.1073/pnas.64.3.1079

[37]Klugkist, J., Voorberg, J., Haaker, H., and Veeger, C. (**1986**) Characterization of three different flavodoxins from *Azotobacter vinelandii Eur. J. Biochem.* 155, 33– 40, DOI: 10.1111/j.1432-1033.1986.tb09455.x

[38]Steensma, E., Heering, H. A., Hagen, W. R., and Van Mierlo, C. P. M. (**1996**) Redox properties of wild-type, Cys69Ala, and Cys69Ser *Azotobacter vinelandii* flavodoxin II as measured by cyclic voltammetry and EPR spectroscopy *Eur. J. Biochem.* 235, 167– 172, DOI: 10.1111/j.1432-1033.1996.00167.x

[39]Lanzilotta, W. N., Ryle, M. J., and Seefeldt, L. C. (**1995**) Nucleotide hydrolysis and protein conformational changes in *Azotobacter vinelandii* nitrogenase iron protein: Defining the function of aspartate 129 *Biochemistry* 34, 10713– 10723, DOI: 10.1021/bi00034a003

[40]Jacobs, D. and Watt, G. D. (**2013**) Nucleotide-assisted [Fe_4S_4] redox state interconversions of the *Azotobacter vinelandii* Fe protein and their relevance to nitrogenase catalysis *Biochemistry* 52, 4791– 4799, DOI: 10.1021/bi301547b

[41]Christiansen, J., Goodwin, P. J., Lanzilotta, W. N., Seefeldt, L. C., and Dean, D. R. (**1998**) Catalytic and biophysical properties of a nitrogenase Apo-MoFe protein produced by a *nif*B-deletion mutant of *Azotobacter vinelandii Biochemistry* 37, 12611– 12623, DOI: 10.1021/bi981165b

[42]Barney, B. M., Igarashi, R. Y., Dos Santos, P. C., Dean, D. R., and Seefeldt, L. C. (**2004**) Substrate interaction at an iron-sulfur face of the FeMo-cofactor during nitrogenase catalysis *J. Biol. Chem.* 279, 53621– 53624, DOI: 10.1074/jbc.M410247200

[43]Brune, M., Hunter, J. L., Corrie, J. E. T., and Webb, M. R. (**1994**) Direct, real-time measurement of rapid inorganic phosphate release using a novel fluorescent probe and its application to actomyosin subfragment 1 ATPase *Biochemistry* 33, 8262– 8271, DOI: 10.1021/bi00193a013

[44]Maaty, W. S., Selvig, K., Ryder, S., Tarlykov, P., Hilmer, J. K., Heinemann, J., Steffens, J., Snyder, J. C., Ortmann, A. C., Movahed, N., Spicka, K., Chetia, L., Grieco, P. A., Dratz, E. A., Douglas, T., Young, M. J., and Bothner, B. (**2012**) Proteomic analysis of *Sulfolobus solfataricus* during *Sulfolobus* turreted icosahedral virus infection *J. Proteome Res.* 11, 1420– 1432, DOI: 10.1021/pr201087v

[45]Vaudel, M., Burkhart, J. M., Zahedi, R. P., Oveland, E., Berven, F. S., Sickmann, A., Martens, L., and Barsnes, H. (**2015**) PeptideShaker enables reanalysis of MS-derived proteomics data sets *Nat. Biotechnol.* 33, 22– 24, DOI: 10.1038/nbt.3109

[46]Johnson, J. L., Nyborg, A. C., Wilson, P. E., Tolley, A. M., Nordmeyer, F. R., and Watt, G. D. (**2000**) Analysis of steady state Fe and MoFe protein interactions during nitrogenase catalysis *Biochim. Biophys. Acta,*

Protein Struct. Mol. Enzymol. 1543, 24– 35, DOI: 10.1016/S0167-4838(00)00195-3

[47]Watt, G. D. and Reddy, K. R. N. (**1994**) Formation of an all ferrous Fe_4S_4 cluster in the iron protein component of *Azotobacter vinelandii* nitrogenase *J. Inorg. Biochem.* 53, 281– 294, DOI: 10.1016/0162-0134(94)85115-8

[48]Lanzilotta, W. N. and Seefeldt, L. C. (**1997**) Changes in the midpoint potentials of the nitrogenase metal centers as a result of iron protein–molybdenum-iron protein complex formation *Biochemistry* 36, 12976–12983, DOI: 10.1021/bi9715371

[49]Johnson, J. L., Tolley, A. M., Erickson, J. A., and Watt, G. D. (**1996**) Steady-state kinetic studies of dithionite utilization, component protein interaction, and the formation of an oxidized iron protein intermediate during *Azotobacter vinelandii* nitrogenase catalysis *Biochemistry* 35, 11336– 11342, DOI: 10.1021/bi952581o

[50]Lowery, R. G. and Ludden, P. W. (**1988**) Purification and properties of dinitrogenase reductase ADP-ribosyltransferase from the photosynthetic bacterium *Rhodospirillum rubrum J. Biol. Chem.* 263, 16714– 16719

[51]Moure, V. R., Danyal, K., Yang, Z.-Y., Wendroth, S., Müller-Santos, M., Pedrosa, F. O., Scarduelli, M., Gerhardt, E. C. M., Huergo, L. F., Souza, E. M., and Seefeldt, L. C. (**2013**) The nitrogenase regulatory enzyme dinitrogenase reductase ADP-ribosyltransferase (DraT) is activated by direct interaction with the signal transduction protein GlnB *J. Bacteriol.* 195, 279– 286, DOI: 10.1128/JB.01517-12

[52]Seefeldt, L. C. and Dean, D. R. (**1997**) Role of nucleotides in nitrogenase catalysis *Acc. Chem. Res.* 30, 260– 266, DOI: 10.1021/ar960260e

[53]Wong, E. V., Cao, W., Vörös, J., Merchant, M., Modis, Y., Hackney, D. D., Montpetit, B., and De La Cruz, E. M. (**2016**) Pi release limits the intrinsic and RNA-stimulated ATPase cycles of DEAD-box protein 5 (Dbp5) *J. Mol. Biol.* 428, 492– 508, DOI: 10.1016/j.jmb.2015.12.018

[54]Wang, Q., Arnold, J. J., Uchida, A., Raney, K. D., and Cameron, C. E. (**2010**) Phosphate release contributes to the rate-limiting step for unwinding by an RNA helicase *Nucleic Acids Res.* 38, 1312– 1324, DOI: 10.1093/nar/gkp1118

[55]Cochran, J. C., Krzysiak, T. C., and Gilbert, S. P. (**2006**) Pathway of ATP hydrolysis by monomeric kinesin Eg5 *Biochemistry* 45, 12334– 12344, DOI: 10.1021/bi0608562

[56]Lionne, C., Iorga, B., Candau, R., Piroddi, N., Webb, M. R., Belus, A., Travers, F., and Barman, T. (**2002**) Evidence that phosphate release is the rate-limiting step on the overall ATPase of psoas myofibrils prevented from shortening by chemical cross-linking *Biochemistry* 41, 13297– 13308, DOI: 10.1021/bi0260278

[57]Lionne, C., Brune, M., Webb, M. R., Travers, F., and Barman, T. (**1995**) Time resolved measurements show that phosphate release is the rate limiting step on myofibrillar ATPases *FEBS Lett.* 364, 59– 62, DOI: 10.1016/0014-5793(95)00356-E

[58]Milic, B., Andreasson, J. O. L., Hancock, W. O., and Block, S. M. (**2014**) Kinesin processivity is gated by phosphate release *Proc. Natl. Acad. Sci. U. S. A.* 111, 14136– 14140, DOI: 10.1073/pnas.1410943111